Video Article

Dependence of Laser-induced Breakdown Spectroscopy Results on Pulse Energies and Timing Parameters Using Soil Simulants

Lauren Kurek[1], Maya L. Najarian[1], David A. Cremers[2], Rosemarie C. Chinni[1]

[1]Department of Math and Sciences, Alvernia University

[2]Applied Research Associates (ARA), Inc.

Correspondence to: Rosemarie C. Chinni at Rosemarie.Chinni@alvernia.edu

URL: http://www.jove.com/video/50876
DOI: doi:10.3791/50876

Keywords: Chemistry, Issue 79, analytical chemistry, laser research, atomic physics, [LIBS, Laser-induced breakdown spectroscopy, gated and non-gated detection, energy study]

Date Published: 9/23/2013

Citation: Kurek, L., Najarian, M.L., Cremers, D.A., Chinni, R.C. Dependence of Laser-induced Breakdown Spectroscopy Results on Pulse Energies and Timing Parameters Using Soil Simulants. *J. Vis. Exp.* (79), e50876, doi:10.3791/50876 (2013).

Abstract

The dependence of some LIBS detection capabilities on lower pulse energies (<100 mJ) and timing parameters were examined using synthetic silicate samples. These samples were used as simulants for soil and contained minor and trace elements commonly found in soil at a wide range of concentrations. For this study, over 100 calibration curves were prepared using different pulse energies and timing parameters; detection limits and sensitivities were determined from the calibration curves. Plasma temperatures were also measured using Boltzmann plots for the various energies and the timing parameters tested. The electron density of the plasma was calculated using the full-width half maximum (FWHM) of the hydrogen line at 656.5 nm over the energies tested. Overall, the results indicate that the use of lower pulse energies and non-gated detection do not seriously compromise the analytical results. These results are very relevant to the design of field- and person-portable LIBS instruments.

Video Link

The video component of this article can be found at http://www.jove.com/video/50876/

Introduction

Laser-induced breakdown spectroscopy (LIBS) is a simple method of elemental analysis that uses a laser-generated spark as the excitation source. The laser pulse is focused onto a surface that heats, ablates, atomizes and ionizes the surface material resulting in the formation of plasma. The plasma light is spectrally resolved and detected and elements are identified by their spectral signatures. If properly calibrated, LIBS can provide quantitative results. LIBS can analyze solids, gases, and liquids with little or no sample preparation.[1] These characteristics make it ideal for analyses that cannot be carried out in the laboratory.

Currently, LIBS is being studied for many different applications especially those that require field-based measurements for quantification.[1-8] This requires the development of LIBS instrumentation using rugged and compact components suitable for a field-based system. In most cases, these components will not have the full capabilities of laboratory-based instrumentation, thereby compromising the analysis performance. LIBS results are dependent on laser pulse parameters and other measurement conditions that include sampling geometry, surrounding atmosphere, and the use of gated or non-gated detection.[9-12] For field-based LIBS instrumentation, two important factors to consider are the pulse energy and the use of gated versus non-gated detection. These two factors determine to a large extent the cost, size, and complexity of the LIBS instrument. Small, ruggedly built lasers that can generate pulses from 10-50 mJ at repetition rates of 0.3-10 Hz are commercially available and would be highly advantageous to use. Therefore, it is important to know what, if any, loss in detection capabilities will result from the use of these lasers. The pulse energy is a key parameter for LIBS as it determines the amount of material ablated and vaporized and the excitation characteristics of the plasma. In addition, the use of gated detection can increase the cost of the LIBS system; as a result, it is imperative to determine the differences between spectra and detection capabilities using gated and non-gated detection.

Recently, a study was performed comparing gated detection to non-gated detection for minor elements found in steel. The results showed that the detection limits were comparable if not better for non-gated detection.[12] One important characteristic of LIBS is that the technique experiences physical and chemical matrix effects. An example of the former is that the laser pulse couples more efficiently with conducting/metal surfaces than non-conducting surfaces.[13] For this study, we wanted to determine the effects of pulse energy and timing parameters for non-conducting materials like soil simulants.

Although, field portable LIBS instruments have been developed and used for some applications, a comprehensive study on the detection capabilities has not been performed comparing higher energy and gated systems to lower energy and non-gated systems using soil simulants. This study focuses on laser pulse energy and timing parameters for determination of trace elements in complex matrices. The laser pulse energy ranged from 10 to 100 mJ to obtain a comparison between lower and higher energies. A comparison of the use of gated versus non-gated detection was also performed over the same energy range.

Protocol

1. Laser System

1. Use laser pulses produced by a Q-switched Nd:YAG laser operating at 1,064 nm and at 10 Hz.
2. Focus the laser pulses onto the sample with a 75 mm focal length lens.
3. Collect the plasma light with an optical fiber pointed at and placed near the plasma formed on the sample.
4. Use an Echelle spectrograph/ICCD to spectrally resolve and record the LIBS spectrum.
5. Operate the ICCD in both non-gated and gated modes using a gain of 125.
6. Use a 0 µsec time delay (t_d) in non-gated mode and a 1 µsec t_d in gated mode.
7. For both modes, use a gate width (t_b) of 20 µsec with a 3 sec exposure (integrating the plasma light on the ICCD camera chip); this will result in 30 individual laser shots being added to produce each spectrum.
8. Record a total of 5 such spectra for each sample analyzed.
9. Use a digital delay generator to control the timing between the laser and the ICCD gate pulse. The experimental set up is shown in **Figure 1**.
10. Verify the timing with an oscilloscope.
11. Operate the laser at pulse energies of 10, 25, 50, and 100 mJ using both non-gated and gated detection.
12. Continually monitor the laser energy and adjust to correct for drift, if necessary.
13. Safety Consideration: The Nd:YAG laser is a Class IV laser; wear appropriate laser safety goggles at all times when operating the laser and establish room interlocks in conjunction with the room door and laser.[14]

2. Samples and Sample Preparation

1. Use synthetic silicate certified reference materials with known element concentrations as samples; these mimic common soil samples with minor and trace amounts of selected elements spanning a range of concentrations.
2. Concentrations of the trace elements ranged from a few ppm to 10,000 ppm. **Table 1** lists the elements monitored here including their line types and wavelengths used for analysis. The line types labeled as I and II signify neutral atoms or a singly ionized atoms, respectively. The common base composition of each silicate sample is SiO_2 (72%), Al_2O_3 (15%), Fe_2O_3 (4%), $CaMg(CO_3)_2$ (4%), Na_2SO_4 (2.5%), and K_2SO_4 (2.5%).
3. Press the samples into 31 mm diameter pellets using a hydraulic press to create a smooth surface for LIBS analysis. The smooth surface helps to create consistency with the LIBS results.
4. Analyze a new sample spot for each spectrum recorded.
5. Safety consideration: The synthetic silicate samples contain a wide variety of elements at various concentrations; wear gloves during handling.

3. Preparing Calibration Curves

1. Prepare calibration curves for the various elements in both gated and non-gated detection over the range of laser energies tested.
2. Make these curves by plotting the peak area or the ratioed peak area (y-axis) against element concentration (x-axis).
3. Use a linear trend line to fit the calibration curve. [screen shot 1]
4. Calculate detection limits using 3σ detection as defined by IUPAC.[15] [calculation 1]

4. Plasma Temperature Determination

1. Measure plasma temperatures from Boltzmann plots.
2. Use a set of iron lines [Fe(I)] between wavelengths of 371-408 nm to create Boltzmann plots using: $\ln(I\lambda/gA) = -E_u/kT - \ln(4\rho Z/hcN_0)$ (Eq. 1) where I is the intensity of the transition as determined from the peak area, λ is the wavelength, A is the transition probability, g is the degeneracy of the transition, E_u is the upper state for emission, k is the Boltzmann constant, T is the temperature, Z is the partition function, h is Planck's constant, c is the speed of light, N_0 is the total species population.
3. Chose Fe lines that have known E_u, g, and A values.

- The Fe(I) lines used here are 371.99, 374.56, 382.04, 404.58, 406.36 nm.
- The E_u, g, and A values can be found on this website (http://physics.nist.gov/PhysRefData/ASD/lines_form.html)
- Make sure to select the option to show the "g" under additional criteria labeled as level information.
- Use the E_k and g_k values.

4. To determine temperature, plot $\ln(I\lambda/gA)$ against E_u and fit the data with a linear trend line; the slope is equals to -1/kT.[16,17] [screen shot 2]

5. Electron Density Determination

1. To measure the electron density, use the full width at half maximum (FWHM) of the hydrogen line at 656.5 nm.
2. Take this data using t_d=0.5 µsec and t_b= 4.5 µsec on the ICCD.
3. Measure the FWHM of the hydrogen line. [screen shot 3]
4. Calculate the electron density using: $N_e = 8.02 \times 10^{12}[\Delta\lambda_{1/2}/\alpha_{1/2}]^{3/2}$ (Eq. 2) where N_e is the electron density, $\Delta\lambda_{1/2}$ is the measured FWHM of the hydrogen line, and $\alpha_{1/2}$ is the reduced wavelength which is a function of the temperature and the electron density. The values for the reduced wavelengths are provided in Griem's Appendix IIIa.[16-18]

5. Calculate the electron density using a temperature of 10,000 K (this was the close to the average temperature of the plasma). [screen shot 4]

6. Work up All Data Using a Program that Can Determine the Peak Areas and/or Microsoft Excel

Representative Results

Effect of laser pulse energy and detection modes on detection capabilities. LIBS spectra of the synthetic silicate samples were recorded using gated and non-gated detection over the range of laser pulse energies tested. Over 100 calibration curves were constructed from these data to evaluate the effect of the laser pulse energy. Calibration curves were prepared by (1) using the area under the analyte peak and (2) by ratioing the area of the analyte peak to the area of the iron peak at 405.58 nm. The iron concentration was uniform between samples; therefore, it was used as an internal standard. Ratioing the analyte area to the area of an internal standard element may increase the measurement reproducibility especially if there are shot-to-shot laser energy fluctuations. The detection sensitivity (calibration curve slope) and detection limit data using both non-gated and gated detection modes are shown in **Tables 2, 3, 4, and 5**.

For all elements, using the unratioed calibration curves for both gated and non-gated detection, there was a direct correlation between laser pulse energy and the sensitivity: sensitivity increased with energy. Therefore, the analyte signals were larger at the higher pulse energies since sensitivity is dependent on the analyte signal relative to its concentration. These results indicate that higher pulse energies might be useful for increasing weak analyte signals. In general, when comparing the ratioed sensitivity data for non-gated detection, there was a slight decrease in sensitivity as the energy was increased; this is most likely due to the higher background in the LIBS spectrum and is discussed in the section labeled "effect of laser energy and detection modes on spectra." However, when comparing the ratioed sensitivity data for gated detection, the sensitivities were relatively constant over the range of energies tested, as expected. This is due to the fact that when the analyte peak areas are ratioed to an area of an element that is at a constant concentration, there is an internal correction taking place that keeps the ratioed elemental areas relatively the constant. These data are shown in **Tables 2 and 3**.

In contrast to the results obtained for the sensitivity in the unratioed data, generally, there was not a correlation between detection limit and laser pulse energy; this is expected since the detection limit depends on both sensitivity and the signal reproducibility (**Table 4**). When comparing the ratioed data to the non-ratioed data for both gated and non-gated detection, the ratioed data predominantly exhibited lower detection limits and generally produced better linear correlations than the non-ratioed data; these results indicate that an internal standard may be used to provide lower detection limits (**Tables 4 and 5**). The ratioed data also showed lower percent relative standard deviations than the non-ratioed data; this directly correlates with the detection limit results being lower for the ratioed data than the non-ratioed data.

Further examination of the non-gated detection results showed that at the higher laser pulse energies, some of the elements showed no correlation ($R^2 < 0.7$); this mainly affected the determination of lead and manganese. Since there was a more intense plasma at higher energies, some of the spectral lines were slightly obscured with non-gated detection at the higher pulse energies due to the high background of the continuum in the LIBS spectrum; this higher background most likely caused the poor linear correlations with lead and manganese. This background is further explained in the "effect of laser energy and detection modes on spectra" section below. Additionally, there were a few instances with the results for non-gated detection limits where no correlation was observed for the unratioed data but a correlation was obtained from the ratioed data. From this, we can conclude that ratioing the elemental signal to another element helps to improve correlations using the unratioed elemental signals. Overall, the process of ratioing the area of the analyte element to the area of an internal standard element appeared to provide a correction for some fluctuations in signals due to coupling differences with laser pulse and the sample; this was observed with the better linear correlations of the ratioed data.

Effect of laser energy and detection modes on spectra. As is well known, spectra recorded using gated detection show a lower baseline when compared to spectra taken using non-gated mode. This can be seen when comparing spectra of a synthetic silicate sample GBW 07709 using gated and non-gated detection at 10 mJ/pulse in **Figures 2a and b**. No self-absorption was observed in the spectra using gated detection over the range of pulse energies tested. The peak areas of the elements in the synthetic silicate samples increased as laser pulse energy was increased for gated detection; this is most likely due to a greater mass of sample ablated and a larger plasma resulting in stronger excitation. Similar results were obtained for non-gated detection showing, in general, an increase in signal as the pulse energy was increased. These results can be seen in **Figure 3** for aluminum, magnesium, and calcium neutral and ionized lines.

Figure 4 further shows that the background clearly increases as the laser energy was increased for non-gated detection. This caused the spectral lines in certain regions to become wider and less intense and is most likely due to self-absorption and an increased background caused by the plasma continuum. This could further affect the detection capabilities at higher energies and is the most probable reason as to why there was no correlation at the higher laser energies using non-gated detection. To avoid this issue, it would be best to use lower pulse energies with non-gated detection.

Effect of laser energy and detection modes on temperature and electron density. Using the Boltzmann plots, the average temperature of the plasma formed on a simulant sample was determined as a function of laser energy for both continuous and gated modes of detection. A typical Boltzmann plot is shown in **Figure 5**. The results show that the temperature of the plasma was relatively constant over the range of energies tested for both detection modes. The plasma temperatures ranged from 10,000-11,000 K in non-gated mode and 8,100 to 8,700 K in gated mode. Non-gated mode operation produced slightly higher temperatures; this is reasonable because the earliest part of the plasma formation is monitored in non-gated mode.

The average electron density of the plasma was measured using the FWHM of the hydrogen line at 656.2 nm and a time delay of 0.5 µsec with a gate width of 4.5 µsec. The hydrogen line could originate from both the air and the synthetic silicate sample. Sufficient hydrogen signal was obtained at all energies tested. The electron density increased with energy from 1.5-2.0 x 10^{17} cm^{-3}, indicating a minor increase in electron density over a 10-fold increase in energy.

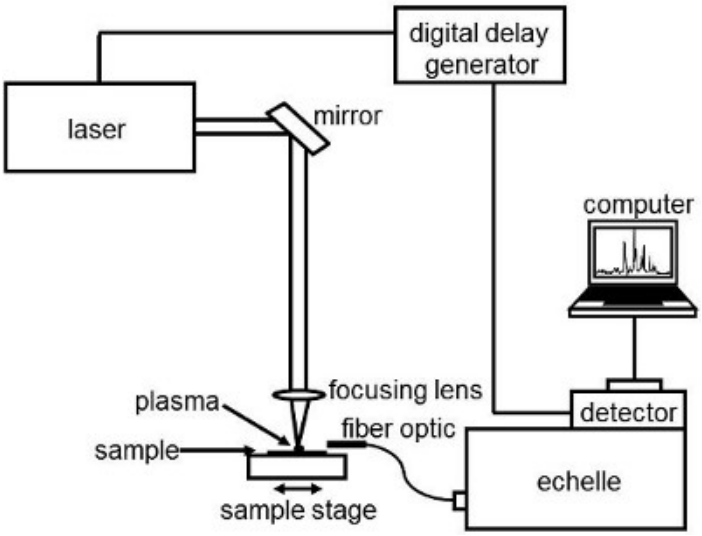

Figure 1. A diagram of the LIBS setup. This shows the general setup for the LIBS experiment used for this analysis.Click here to view larger image.

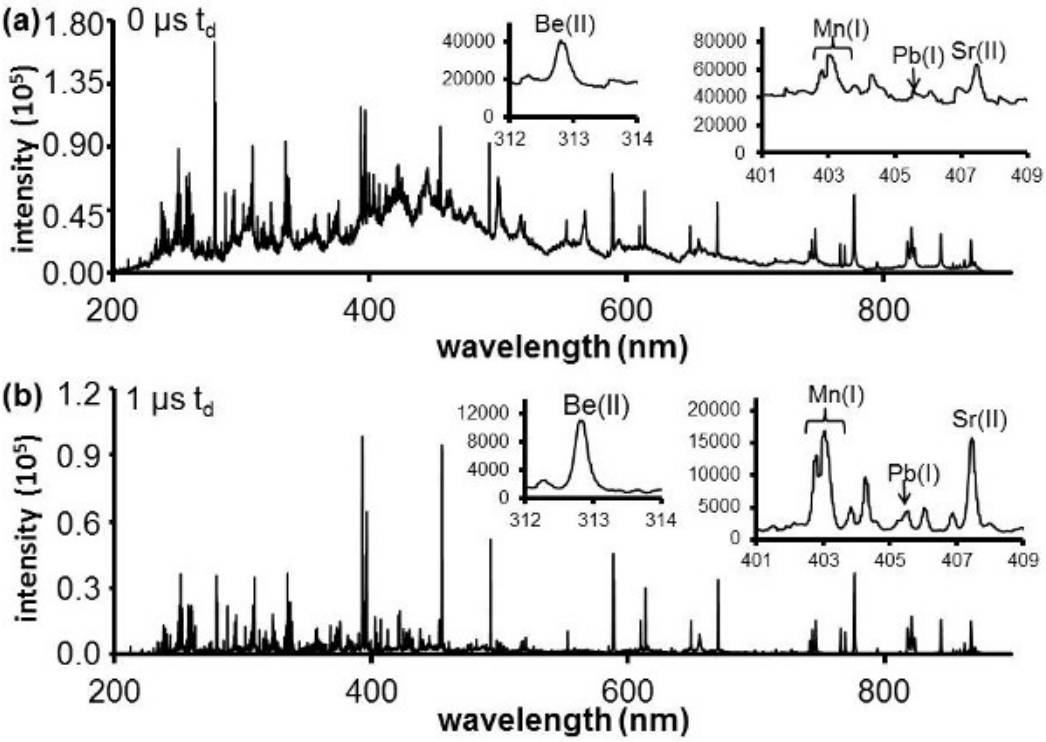

Figure 2. A typical LIBS spectrum (10 mJ) of synthetic silicate sample 07709 (a) using gated detection of 0 µsec time delay and a 20 µsec gate width and (b) using non-gated detection of 1 µsec time delay and a 20 µsec gate width. Click here to view larger image.

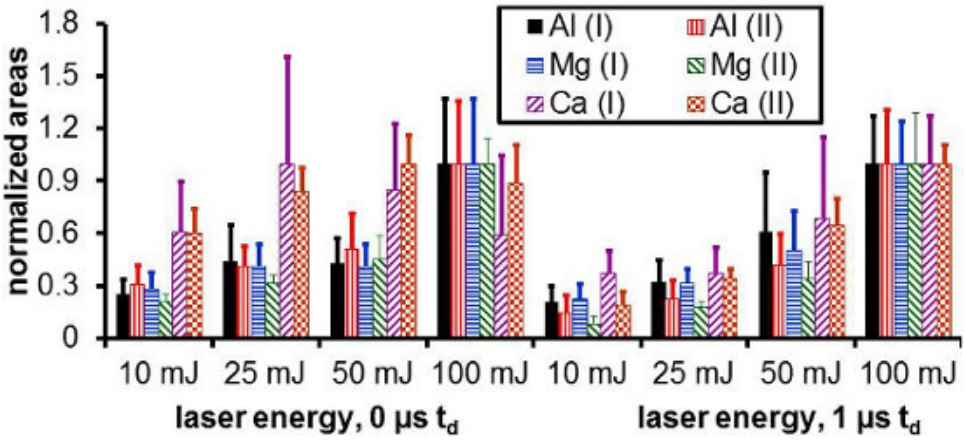

Figure 3. A comparison of normalized peak areas for Al(I), Al(II), Mg(I), Mg(II), Ca(I), and Ca(II) in the synthetic silicate sample 07709 over the range of energies tested for both non-gated (t_d =0 µsec) and gated detection (t_d =1 µsec). Click here to view larger image.

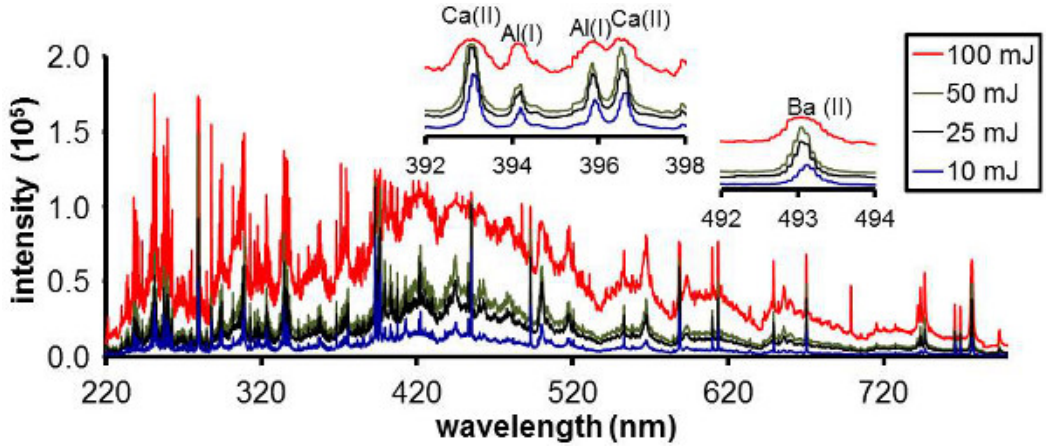

Figure 4. The LIBS spectra for synthetic silicate sample 07709 using non-gated detection at 10, 25, 50, and 100 mJ. Click here to view larger image.

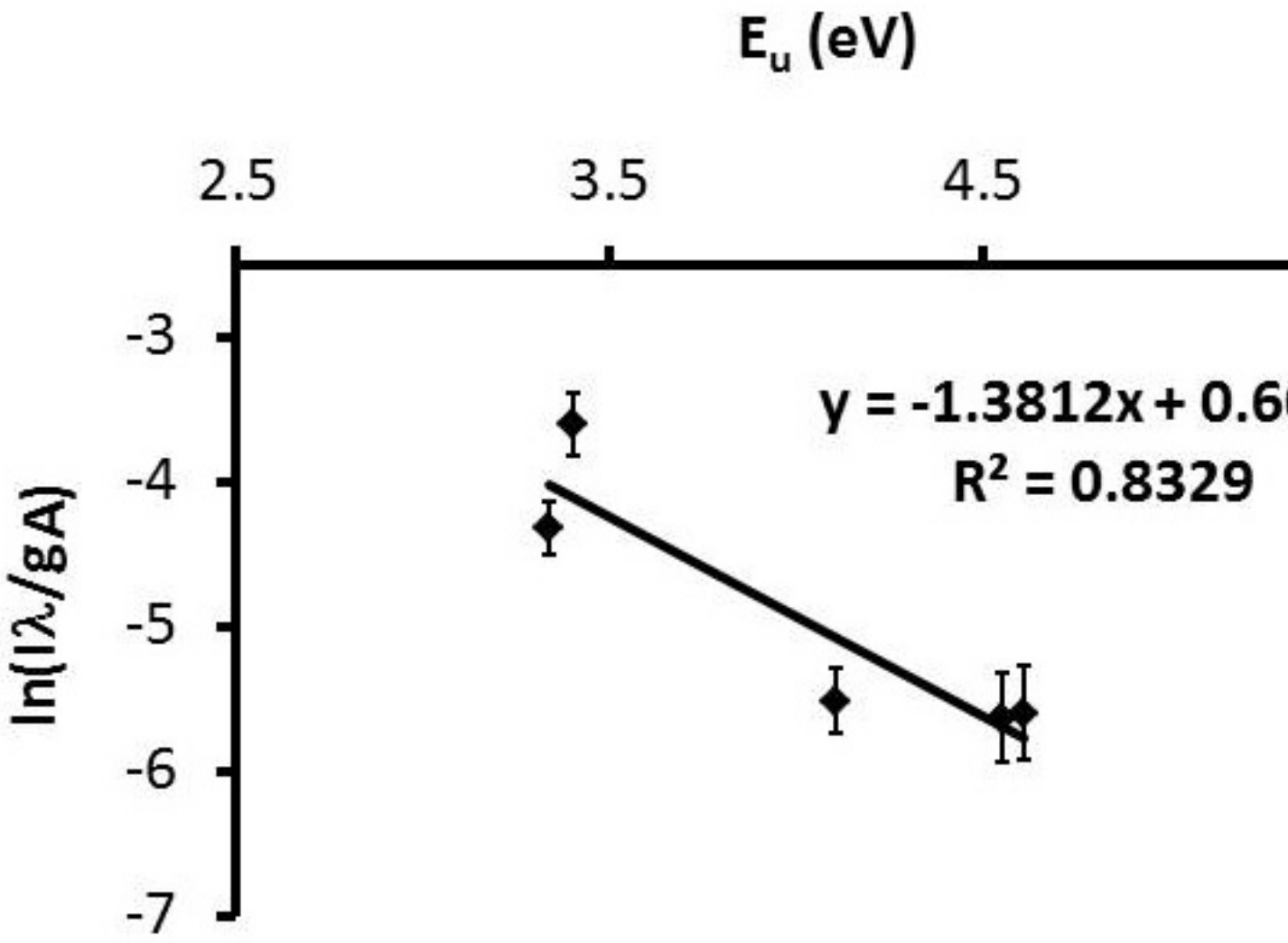

Figure 5. A typical Boltzmann plot. This data comes from using 25 mJ of energy with a 1 µsec time delay. Each point represents an average of five trials. Click here to view larger image.

Element	Line type	Wavelength (nm)
Ba	(II)	493.41
Be*	(II)	313.04, 313.11
Fe**	(I)	404.58
Pb	(I)	405.78
Li*	(I)	670.78, 670.79
Mn*	(I)	403.08, 403.31, 403.45
Sr	(II)	407.77
Ti	(II)	334.94

Table 1. Spectral information for the elements analyzed in the synthetic silicate samples. This table contains the elemental symbol, line type, and the wavelength(s) used for the analysis. *For these elements the closely-spaced lines were not resolved. In this case, the total area under the unresolved lines was determined. **Fe was at constant concentration in the synthetic silicate samples; this element was used to ratio the other analyte peak areas.

Sensitivities* (x10^4 ppm^{-1}) *for Ratioed Data using a 0 µsec t_d				
	10 mJ	**25 mJ**	**50 mJ**	**100 mJ**
Ba	11	9.0	8.3	5.0
Be	340	210	200	230
Li	63	60	69	39
Mn	6.0	4.7	4.1	N.C.
Pb	6.1	N.C.	1.0	N.C.
Sr	38	27	24	16
Ti	7.7	2.0	5.7	4.5
Sensitivities for Unratioed Data using a 0 µsec t_d				
	10 mJ	**25 mJ**	**50 mJ**	**100 mJ**
Ba	38	68	80	90
Be	1200	1500	2100	4400
Li	N.C.	400	N.C.	660
Mn	17	34	N.C.	N.C.
Pb	21	N.C.	N.C.	N.C.
Sr	130	210	N.C.	290
Ti	27	46	55	81

Table 2. Sensitivities for the 0 µsec time delay data. These were obtained from the slopes of the linear calibration curves for various elements using non-gated (t_d = 0 µsec) detection over the range of energies tested. For the ratioed sensitivities, the analyte elemental area was ratioed to a Fe (I) line. N.C. = no correlation: $R^2 < 0.7$.

Sensitivities (x10M^4 ppm^{-1}) for Ratioed Data using a 1 µs t_d				
	10 mJ	**25 mJ**	**50 mJ**	**100 mJ**
Ba	9.9	10	10	8.4
Be	110	100	170	140
Li	72	59	67	52
Mn	5.6	5.2	5.1	4.8
Pb	6.8	7.9	6.9	7.4
Sr	33	30	31	27
Ti	3.7	4.3	5.0	4.9
Sensitivities for Unratioed Data using a 1 µs t_d				
	10 mJ	**25 mJ**	**50 mJ**	**100 mJ**
Ba	30	60	98	140
Be	330	600	1700	2500
Li	220	720	1100	1600
Mn	16	30	49	80
Pb	21	48	72	130
Sr	100	180	310	480
Ti	11	25	48	84

Table 3. Sensitivities for the 1 µs time delay data. These were obtained from the slopes of the linear calibration curves for various elements using gated (t_d = 1 µs) detection over the range of energies tested. For the ratioed sensitivities, the analyte elemental area was ratioed to a Fe (I) line.

Detection Limits for Ratioed Data using a 0 µsec t_d				
	10 mJ	**25 mJ**	**50 mJ**	**100 mJ**
Ba	310 (0.99)	310 (0.99)	280 (0.99)	610 (0.96)
Be	2.1 (0.99)	6.7 (0.99)	3.7 (0.99)	4.8 (0.89)
Li	170 (0.98)	48 (0.97)	87 (0.98)	100 (0.78)
Mn	710 (0.99)	1400 (0.99)	820 (0.99)	N.C.
Pb	250 (0.97)	N.C.	3200 (0.85)	N.C.
Sr	60 (0.99)	70 (0.99)	50 (0.99)	32 (0.96)
Ti	310 (0.99)	690 (0.97)	500 (0.99)	250 (0.89)
Detection Limits for Unratioed Data using a 0 µsec t_d				
	10 mJ	**25 mJ**	**50 mJ**	**100 mJ**
Ba	660 (0.92)	450 (0.99)	480 (0.76)	830 (0.93)
Be	5.6 (0.97)	9.9 (0.99)	5.5 (0.77)	6.5 (0.84)
Li	N.C.	160 (0.91)	N.C.	220 (0.76)
Mn	2900 (0.79)	1500 (0.98)	N.C.	N.C.
Pb	1000 (0.88)	N.C.	N.C.	N.C.
Sr	230 (0.93)	100 (0.99)	N.C.	60 (0.92)
Ti	800 (0.94)	770 (0.99)	530 (0.71)	1100 (0.92)

Table 4. Detection Limit Data for a 0 µsec time delay. The detection limit data are shown in ppm using a 0 µsec time delay over the various laser energies showing both ratioed and unratioed data. The linear graph correlations (R^2) are in parentheses. N.C. means no correlation was observed ($R^2 < 0.7$). For the ratioed sensitivities, the analyte elemental area was ratioed to a Fe (I) line.

Detection Limits for Ratioed Data using a 1 µsec t_d				
	10 mJ	**25 mJ**	**50 mJ**	**100 mJ**
Ba	93 (0.99)	170 (0.99)	160 (0.99)	170 (0.99)
Be	2.5 (0.99)	1.5 (0.99)	1.9 (0.99)	2.1 (0.99)
Li	78 (0.98)	82 (0.91)	62 (0.92)	130 (0.95)
Mn	250 (0.96)	280 (0.99)	220 (0.97)	370 (0.98)
Pb	53 (0.99)	160 (0.99)	91 (0.99)	120 (0.98)
Sr	21 (0.99)	15 (0.99)	28 (0.99)	11 (0.99)
Ti	280 (0.97)	290 (0.99)	120 (0.99)	150 (0.99)
Detection Limits for Unratioed Data using a 1 µsec t_d				
	10 mJ	**25 mJ**	**50 mJ**	**100 mJ**
Ba	760 (0.86)	280 (0.82)	190 (0.96)	340 (0.86)
Be	5.1 (0.89)	2.1 (0.87)	2.9 (0.99)	4.7 (0.92)
Li	220 (0.78)	52 (0.86)	100 (0.88)	260 (0.89)
Mn	1200 (0.72)	460 (0.74)	470 (0.89)	1300 (0.81)
Pb	100 (0.88)	170 (0.79)	150 (0.97)	130 (0.84)
Sr	83 (0.89)	18 (0.84)	44 (0.99)	26 (0.86)
Ti	1400 (0.77)	370 (0.79)	290 (0.97)	370 (0.88)

Table 5. Detection Limit Data for a 1 µsec time delay. The detection limit data are shown using a 1 µsec time delay over the various laser energies showing both ratioed and unratioed data. The linear graph correlations (R^2) are in parentheses. For the ratioed sensitivities, the analyte elemental area was ratioed to a Fe (I) line.

Discussion

When comparing non-gated and gated detection modes, the detection limit data show that the gated detection mode allowed for detection of all of the elements including those that were not seen using higher laser energies in non-gated detection mode. Using gated detection, the initial

high background from the formation of the plasma is not observed and the background is decreased showing the elemental emission better resolved. Furthermore, the detection limits were slightly lower using gated detection.

Generally, there were similar detection limits calculated over the range of energies tested for both gated and non-gated detection. There were a few instances where the detection limits were higher using the higher energies with non-gated detection; this was most likely due to the increased background in the LIBS spectrum.

Since there was not a large change in electron density and plasma temperatures over a 10-fold increase in energy, these factors should not affect the detection capabilities over the laser energies tested. This is consistent with our results showing no large decrease in detection limits with increased pulse energy.

From the data presented, a few conclusions can be made about the use of laser pulse energies of 10-100 mJ and different timing parameters for the determination of trace elements in soil stimulants. Lower energies of 10 and 25 mJ provided similar detection limits to those achieved at 50 and 100 mJ. This showed that the use of lower pulse energies does not significantly degrade detection capabilities and that the use of a lower energy, necessary for person portable LIBS instrumentation, will not diminish the detection capabilities. The results also showed that ratioed data produced lower detection limits than the non-ratioed data. Therefore, the detection capabilities of a compact LIBS system could be improved through the use of an internal standard to help normalize the results.

When comparing the spectra between non-gated and gated detection modes, it was found that spectra recorded using gated detection produced a lower baseline and the elemental emission lines were more clearly resolved for some of the elements. Also, slightly lower detection limits were obtained using gated detection over the laser energies tested. This shows that there will be a slight loss in detection capabilities when using non-gated mode detection for soil simulants used here.

Disclosures

The authors do not have anything to disclose.

Acknowledgements

This work was funded through U.S. Department of Energy, Office of Science.

References

1. Song, K., Lee, Y., & Sneddon, J. Recent developments in instrumentation for laser induced breakdown spectroscopy. *Appl. Spec. Rev*. **37** (1), 89-117 (2002).
2. Yamamoto, K.Y., Cremers, D.A., Foster, L.E., & Ferris, M.J. Detection of Metals in the Environment Using a Portable Laser-Induced Breakdown Spectroscopy Instrument. *Appl. Spec.* **50** (2), 222-233 (1996).
3. Cuñat, J., Fortes, F.J., Cabalín, L.M., Carrasco, F., Simón, M.D., & Laserna, J.J. Man-Portable Laser-Induced Breakdown Spectroscopy System for in Situ Characterization of Karstic Formations. *Appl. Spec.* **62** (11), 1250-1255 (2008).
4. Munson, C.A., Gottfried, J.L., Gibb-Snyder, E., DeLucia, F.C., Gullett, B., & Miziolek, A.W. Detection of indoor biological hazards using the man-portable laser induced breakdown spectrometer. *Appl. Opt.* **47** (31), G48-57 (2008).
5. Multari, R.A., Foster, L.E., Cremers, D.A., & Ferris, M.J. Effect of Sampling Geometry on Elemental Emissions in Laser-Induced Breakdown Spectroscopy. *Appl. Spec.* **50** (12), 1483-1499 (1996).
6. Harmon, R.S., DeLucia, F.C., McManus, C.E., McMillan, N.J., Jenkins, T.F., Walsh, M.E., & Miziolek, A. Laser-induced breakdown spectroscopy - An emerging chemical sensor technology for real-time field-portable, geochemical, mineralogical, and environmental applications. *Appl. Geochem.* **21** (5), 730-747 (2006).
7. Schill, A.W., Heaps, D.A., Stratis-Cullum, D.N., Arnold, B.R., & Pellegrino, P.M. Characterization of near-infrared low energy ultra-short laser pulses for portable applications of laser induced breakdown spectroscopy. *Opt. Express*. **15** (21), 14044-14056 (2007).
8. Fortes, F.J. & Laserna, J.J. The development of fieldable laser-induced breakdown spectrometer: No limits on the horizon. *Spectrochim. Acta Part B*. **65** (12), 975-990 (2010).
9. Leis, F., Sdorra, W., Ko, J.B., & Niemax K. Basic Investigations for Laser Microanalysis: I. Optical Emission Spectrometry of Laser-Produced Sample Plumes. *Mikrochim. Acta II*. **98,** 185-199 (1989).
10. Lida, Y. Effects of atmosphere on laser vaporization and excitation processes of solid samples. *Spectrochim. Acta Part B.* **45** (12), 1353-1367 (1990).
11. Radziemski, L.J. & Loree, T.R. Laser-induced breakdown spectroscopy: Time-integrated applications. *J. Plasma Chem. Plasma Proc.* **1** (3), 281-293 (1981).
12. Mueller, M., Gornushkin, I.B., Florek, S., Mory, D., & Panne, U. Approach to Detection in Laser-Induced Breakdown Spectroscopy. *Anal. Chem.* **79** (12), 4419-4426 (2007).
13. Fan, C. & Longtin, J.P. Modeling Optical Breakdown in Dielectrics During Ultrafast Laser Processing. *Appl. Opt.* **40** (18), 3124-3131 (2001).
14. ANSI Z-136.5, American National Standard for Safe Use of Lasers in Educational Institutions, (2009).
15. Compendium of Chemical Terminology, 2nd ed., IUPAC, Research Triangle Park, NC (1997).
16. Cremers, D.A. & Radziemski, L.J. *Handbook of Laser-Induced Breakdown Spectroscopy*, John Wiley &, Sons, Ltd: Chichester, England (2006).
17. Griem, H.R. *Spectral Line Broadening by Plasmas*, Academic Press: New York, (1974).
18. Ashkenazy, J., Kipper, R., & Caner, M. Spectroscopic Measurements of Electron Density of Capillary Plasma Based on Stark Broadening of Hydrogen Lines. *Phys. Rev. A* **43** (10), 5568-5574 (1991).

